Source geometry from exceptionally high resolution long period event observations at Mt Etna during the 2008 eruption

Louis De Barros,[1] Christopher J. Bean,[1] Ivan Lokmer,[1] Gilberto Saccorotti,[2] Luciano Zuccarello,[1,3] Gareth S. O'Brien,[1] Jean-Philippe Métaxian,[4] and Domenico Patanè[3]

Received 12 October 2009; revised 13 November 2009; accepted 19 November 2009; published 23 December 2009.

[1] During the second half of June, 2008, 50 broadband seismic stations were deployed on Mt Etna volcano in close proximity to the summit, allowing us to observe seismic activity with exceptionally high resolution. 129 long period events (LP) with dominant frequencies ranging between 0.3 and 1.2 Hz, were extracted from this dataset. These events form two families of similar waveforms with different temporal distributions. Event locations are performed by cross-correlating signals for all pairs of stations in a two-step scheme. In the first step, the absolute location of the centre of the clusters was found. In the second step, all events are located using this position. The hypocentres are found at shallow depths (20 to 700 m deep) below the summit craters. The very high location resolution allows us to detect the temporal migration of the events along a dike-like structure and 2 pipe shaped bodies, yielding an unprecedented view of some elements of the shallow plumbing system at Mount Etna. These events do not seem to be a direct indicator of the ongoing lava flow or magma upwelling. **Citation:** De Barros, L., C. J. Bean, I. Lokmer, G. Saccorotti, L. Zuccarello, G. S. O'Brien, J.-P. Métaxian, and D. Patanè (2009), Source geometry from exceptionally high resolution long period event observations at Mt Etna during the 2008 eruption, *Geophys. Res. Lett.*, *36*, L24305, doi:10.1029/2009GL041273.

1. Introduction

[2] Mt Etna is an active 3,330 m high stratovolcano located on the East coast of Sicily, Italy. An eruptive period began on the 10th of May 2008 with a powerful lava fountain in the South East Crater, one of the four main summit craters. An eruptive fracture opened on the 13th of May on the eastern flank of the volcano, in the "Valle del Bove" [see, e.g., *Napoli et al.*, 2008]. The eruption stopped on July 7th 2009.

[3] Long period (LP) events, with frequencies ranging from 0.2 to 1.3 Hz on Mt Etna, are thought to be associated with resonance or transport of fluid in the volcano conduits and are often considered as precursors to an eruption [*Chouet*, 1996]. Locating these events can greatly improve our knowledge of the geometry of the plumbing system of the volcano. Furthermore, an accurate location can help us constrain moment tensor inversions leading to a better understanding of the source process.

[4] As LP signals have an emergent onset, classical travel-time inversion cannot usually be used to locate the source of these events. Several methods have been developed to locate them: semblance method [e.g., *Patanè et al.*, 2008], array techniques with frequency-slowness analysis [*Métaxian et al.*, 2002], amplitude decay [*Battaglia et al.*, 2003], coupled inversion for location and moment tensor [*Kumagai et al.*, 2002] or travel time inversion with improved pick readings achieved through stacking similar events [*Saccorotti et al.*, 2007].

[5] In the past, several studies have been conducted on LP events from Mt Etna [*Falsaperla et al.*, 2002; *Saccorotti et al.*, 2007; *Lokmer et al.*, 2007b; *Patanè et al.*, 2008]. They found LP sources located below the summit area at shallow depths, i.e., 0–2000 m. No rapid changes in the LP source locations were detected, only small changes in the LP event characteristics before and after eruptive periods. The link between LP events and eruptions is still unclear [*Patanè et al.*, 2008]. The location of tremor sources shows two connected dike bodies oriented in a NW–SE direction extending from sea level to the surface [*Patanè et al.*, 2008], which is in agreement with geodetic data [*Bonaccorso et al.*, 2002] and LP source mechanisms [*Lokmer et al.*, 2007a]. However, locations of LP events have not yet shown any clear structural geometry on Mt Etna.

[6] The aim of this paper is to obtain information about LP source distribution. We use the observations from a temporary deployment with 50 broadband stations. LP events were extracted and classified from this dataset. We then focused on the location of these events using the time delays between closely spaced stations measured by cross-correlation. The resulting high resolution source locations show outstanding well-defined geometries with an unprecedented short term temporal variation.

2. Data

[7] A total of 50 stations with three component broadband sensors (30, 40 or 60 s cut-off period with 5 or 10 ms sampling rate) were deployed on Mt Etna volcano between the 18th of June 2008 and the 3rd of July 2008. This included 16 permanent stations from INGV, Italy and 34 temporary stations from University College Dublin (Ireland), Université de Savoie (France) and INGV (Italy). Such a large

[1] School of Geological Sciences, University College Dublin, Dublin, Ireland.
[2] Sezione di Pisa, Istituto Nazionale di Geofisica e Vulcanologia, Pisa, Italy.
[3] Sezione di Catania, Istituto Nazionale di Geofisica e Vulcanologia, Catania, Italy.
[4] LGIT, Université de Savoie, IRD, CNRS, Chambéry, France.

0094-8276/09/2009GL041273$05.00

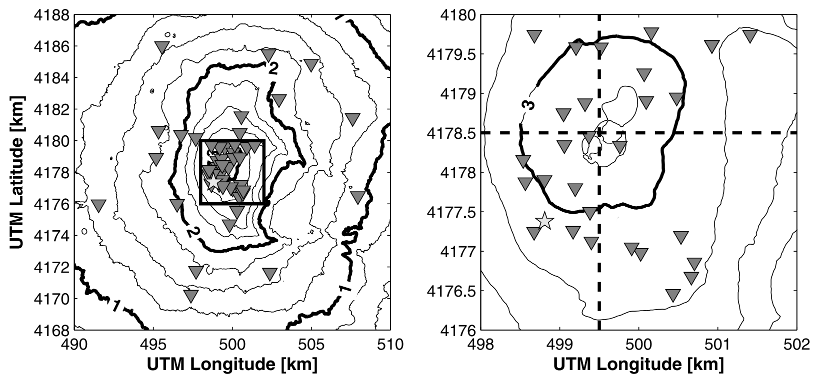

Figure 1. Broadband stations positions. (left) All stations deployed on the volcano. (right) Stations within 2 km of the summit used in this study. Station ECPN is marked by a star. Elevation contour step is 250 m. Thick dotted lines in Figure 1 (right) indicate the positions of the cross-sections used in this study.

number of stations is quite unusual on a volcano. In particular, 30 stations were located within 2 km of the summit area (see Figure 1).

[8] Before analysing the data, we deconvolve the instrument response from the recorded signals. To extract the long period events, we use a STA/LTA method (2 s over 20 s window lengths, with a threshold of 2.5) on the bandpass filtered data (0.2–1.5 Hz), which gives us approximately 500 events. We then classify these events using a cross-correlation analysis between all pairs of signals [*Saccorotti et al.*, 2007]. We keep the events that give a correlation coefficient greater than 0.9 with all events on at least 3 out of the 4 permanent stations close to the summit. We obtain two different families with a similar number of events (63 and 66, respectively).

[9] Figure 2a shows the temporal distribution of these events. The first family is only present in the first two days of the experiment (18th–19th of June), while the second family is distributed over the first four days. After June 22nd, the amplitudes of the LP events decrease by an order of magnitude. In the same period, the tremor amplitude increases. Since both the LPs and tremors are in the same spectral range, it makes it difficult to recognize and extract additional LP events after June 22nd.

[10] The waveforms and the spectral content of the stacked events for both families are shown in Figure 2b. Though the waveforms are quite similar, the spectral peaks are not the same for both families. The second one has a sharper spectrum, with a peak frequency slightly higher than family 1. The waveform similarity within each group suggests spatially close sources with a similar mechanism, while the source position and/or the mechanism have to be different between the two families.

3. Method

[11] The location of the LP events is computed in two steps. We first find the mean position for each family and we then locate the individual events using this first position. As the LPs are emergent (as seen in Figure 2b), it is impossible to directly measure the arrival time. Instead, we choose to use cross-correlation between stations i and j ($i \neq j$) to obtain the time delays t_{ij}^{obs}.

[12] In the first step, we improve the Signal to Noise Ratio by stacking similar events. For a hypothesized source position $X_s(x_s, y_s, z_s)$, we compute the distance between the source and each station. The propagation medium is assumed to be homogeneous which leads to the approximation of spherical wavefronts as the source-to-receiver distances are short. Theoretical time delays $t_{ij}^{th}(X_s)$ between pairs of stations are then obtained by dividing the distance differences by the wave velocity. We then use a grid search to find the position X_s which minimizes the misfit function defined by:

$$R(X_s) = \sum_i \sum_{j \neq i} W_{ij} C_{ij} \left(t_{ij}^{obs} - t_{ij}^{th}(X_s) \right)^2, \qquad (1)$$

where C_{ij} is a weight related to the correlation coefficient $c_{ij}(C_{ij} = [\xi_c/(1 - c_{ij})]^2)$, and W_{ij} a correction factor inversely

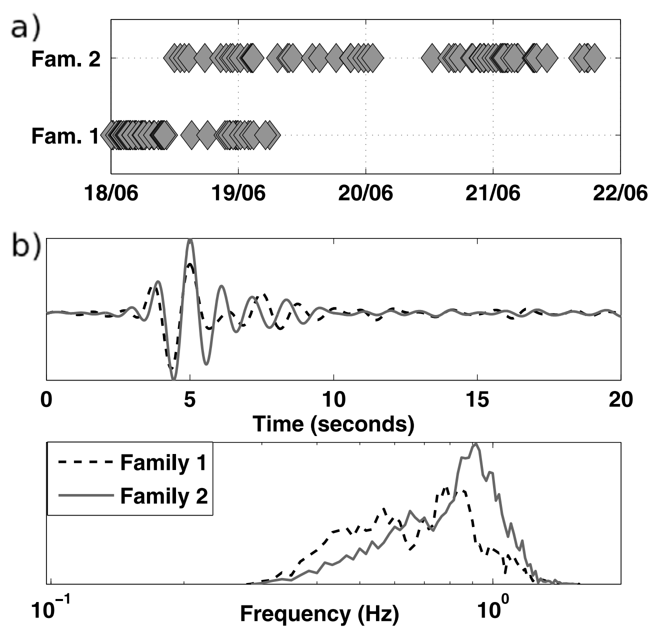

Figure 2. (a) Temporal distribution of the LP events. Families 1 and 2 contain 63 and 66 events, respectively. (b) Waveform and spectral content for stacked events (filtered between 0.2 and 1.5 Hz) at station ECPN (see Figure 1) for both families (Fam 1=dashed line, Fam 2=solid line).

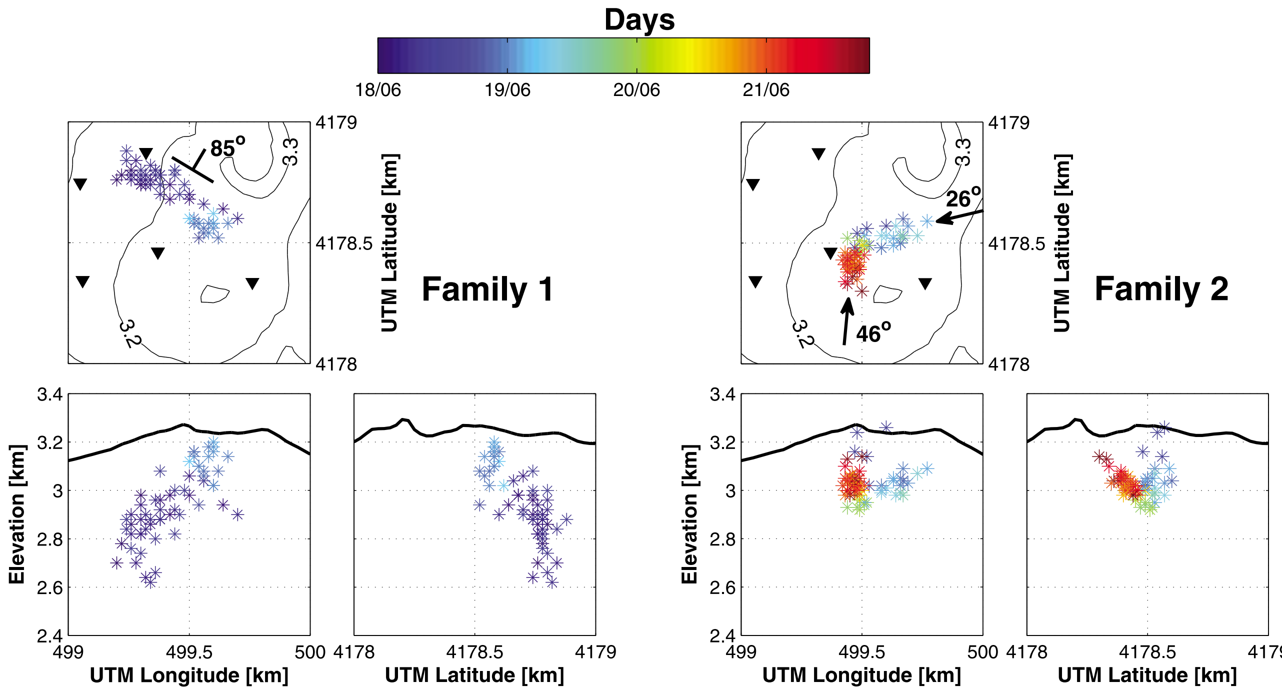

Figure 3. Location of all the LPs for family 1 (left) and 2 (right) with colours indicating temporal evolution. Colourscale (days) is common for both families. Views are from above, South and West. Triangles are some of the broadband stations. The side views correspond to the cross-sections indicated in Figure 1. "⊥" and "→" symbols represent the planar and pipe-shape structures, with dip and plunge angles respectively.

proportional to the time delays between stations ($W_{ij} = \exp[-t_{ij}^{obs^2}/\xi_w]$), as we consider that errors increase with the propagation distance. ξ_c and ξ_w are normalizing constants which can be adjusted.

[13] In this first step, we found the mean location X_0 of the hypocentre for each family. However because individual events are almost monochromatic and quite noisy, one or several cycles can be accidently skipped during the cross-correlation procedure, giving incorrect time delays. To avoid this problem and to refine the grid search, we introduce a second step, locating the individual events in each family using the mean positions of that family as reference positions. We compute the theoretical time delays $t_{ij}^{th}(X_0)$ between each pair of stations using the source position found in the first step. Events are shifted according to this theoretical time, and by cross-correlation we measure the residual time $\delta t_{ij}^{obs} = t_{ij}^{obs} - t_{ij}^{th}(X_0)$. As the source positions are close to each other, this time is much smaller than the central period of the events. The location is then found by minimizing the sum of the squared differences between observed and theoretical residual times for a grid of source position. This involves solving equation (1) in the same manner as in step 1.

[14] Although this location method does account for the topography, it does not take the wave propagation effects (free surface, velocity heterogeneities) into account. However, this is balanced by the large number of stations and their close proximity to the source. Synthetics tests are performed to check the accuracy of the location (see Figure S1 of the auxiliary material).[1] Errors are found to be very small in the horizontal plane (<10 m) and bigger in the vertical direction (<100 m).

4. Location Results

[15] We locate the events for both families with the method from section 3. We only use stations close to the summit, i.e., 25 stations for family 2 and 19 for family 1, according to the available data. We compute the stacked events for both clusters and we use 2 × 2 × 2 km grid with a spacing of 50 m. In order to determine the velocity, we run inversions for wave velocities between 1.2 and 3.2 km/s in steps of 0.2 km/s. The lowest residuals are obtained for a velocity of 1.8 km/s, which is in agreement with near-surface velocity measurements on the Mt Etna [*Patanè et al.*, 2008]. The hypocentre positions are found to be at X_0 = (499.4, 4178.7, 2.95) km for family 1 and X_0 = (499.5, 4178.45, 3) km for family 2. These positions are then used as the reference for the second step. Again we search for the optimum velocity, yielding a value of 1.8 km/s for the shallowest events and 2.2 km/s for the deepest ones. We search for the source positions in a 600 × 600 × 900 m grid with a 10 m spacing. The results of this location procedure are shown in Figure 3.

[16] Firstly, the events for both families are shallow: from 50 to 800 m for family 1 and from 20 to 400 m for family 2. The epicenters of the events are close to the summit craters, and are slightly different for both families. The colourscale in Figure 3 and in Animation S1 of the auxiliary material indicates the origin times of the events. We see that the source positions of family 1 events migrate upwards (but not systematically) from depth to the surface between the 18th and the beginning of the 19th of June. During this

[1]Auxiliary materials are available in the HTML. doi:10.1029/2009GL041273.

Table 1. Main Characteristics of the Structures[a]

Family	ϕ_1 (°)	θ_1 (°)	ϕ_3 (°)	θ_3 (°)	L_1/L_3	L_2/L_3	Strike (°)	Dip (°)
F1	306	46	31	5	5.2	2.5	N301	85E
F2a	254	26	147	42	4.8	1.5	N254	26W
F2b	8	46	172	44	4	1.3	N8	46N

[a]Azimuth (ϕ_1 and ϕ_3) and inclination angle (θ_1 and θ_3) of the major and minor principal parameter axes. Ratio between major (L_1), intermediate (L_2) and minor (L_3) principal parameter axes; strike and dip (=azimuth and plunge for the pipe-shape F2a and F2b).

period, events of family 2 are located in the area occupied by the shallowest events of family 1 and move downwards from the surface to a depth of 400 m. After the middle of June 19th, the hypocentres of family 2 migrate back towards the surface using another path.

[17] To quantify the geometry of the clusters revealed by the hypocentres position, we use a simplified Principal Parameter method [*Michelini and Bolt*, 1986]. The eigenvectors and eigenvalues of the spread matrix (i.e., covariance matrix of the hypocenters) give us the directions and lengths ($L_1 > L_2 > L_3$) of the three principal parameter axes (see Table 1) which allow us to determine the best ellipsoid which fits the source positions. As the cluster geometries are clearly defined, we apply this analysis to the whole of family 1 (F1) and to the two well defined branches (called F2a and F2b in Table 1) of the family 2. The azimuths of the principal axes (noted ϕ_1 and ϕ_3 for major and minor axes) are measured from the north clockwise and corresponding inclination angles θ_1 and θ_3 are from the horizontal plane, positive downward.

[18] Following *Michelini and Bolt* [1986], a planar structure can be defined with $L_1/L_3 \geq 2.5$ and $L_2/L_3 \geq 1.75$. A pipe shape structure will have $L_1/L_3 \geq 2.5$ and $L_1/L_3 < 1.75$. This suggests (see Table 1) that the cluster geometry of family 1 is more dike-like, while the two branches of family 2 are closer to pipe shapes. Family 1 mainly shows a subvertical planar geometry with normal defined by $\phi_3 = 31°$ and $\theta_3 = 5°$. The two clusters of family 2 are elongated in directions $\phi_1 = 74°$, $\theta_1 = 26°$ for F2a and $\phi_1 = 8°$, $\theta_1 = 46°$ for F2b. However, the two clusters F2a and F2b can be merged in a single cluster as they belong to a same plane whose normal is defined by $\phi_3 = 137°$ and $\theta_3 = 37°$. This can be interpreted as the presence of a planar structure for family 2 within which the LP source locations move, branching into two directions.

5. Discussion and Conclusion

[19] Two families of LP events (63 and 66 events selected) were found in the first four days of an experiment carried out between the 18th of June and the 3rd of July, 2008. The data were recorded by an exceptionally high-resolution network, consisting of 50 broadband stations deployed in the close proximity of the source, thus enabling us to locate the source positions with a very high precision. The location of the stacked events and of all the individual events were determined and are on average in broad agreement with previous studies [*Saccorotti et al.*, 2007; *Patanè et al.*, 2008]. However, LP event distributions show outstanding well-defined geometries with an unprecedented temporal evolution. Hypocentres moved, in a 96 hour period, from a depth of 800 m to the surface through a planar structure (family 1 events) which branches at 300 m below the summit craters into two structures which have pipe-like geometries (family 2 events). The deeper structure is subvertical and striking NW–SE (N301°, 85°E) in agreement with the results of *Patanè et al.* [2008] and *Lokmer et al.* [2007a], while the two structures of family 2 are aligned in a SW–NE striking plane (N47°, 53°W). As some events share similar positions but belong to different families, it suggests that the difference between the seismograms comprising the two families is due to the source mechanism.

[20] Mt Etna volcano was active during the experiment with lava flowing from an eruptive fissure on the eastern flank of the volcano. The highest part of the active vents were 500 m below and 1 km from the summit craters. There is no visible evidence of a change in terms of eruptive output associated with the LP migration nor with the energy decrease of the LP events after the 22nd of June. It is clear that these LP events are not representative of the whole eruption, but our results show that the LP activity recorded at this time does not seem to be an indicator of the ongoing flank lava flow nor of magma upwelling. Moreover, the source area and the disappearance of the LP after the 22nd of June can be related to the family 2 events of *Patanè et al.* [2008] which were recorded only for a few weeks after the lava fountains of 2007. This suggests that the events found in this study are more likely the end of the response to the lava fountain of the 10th of May 2008. One possible hypothesis is that these seismic events are associated with magma trapped in plugged conduits leading to the summit craters. Another hypothesis may be that LP events are not directly related to magma, but rather to gas, which is continuously emitted from the summit craters. Determining the source mechanisms by moment tensor inversion [*Kumagai et al.*, 2002; *Lokmer et al.*, 2007a] will provide more insights into the process generating these events.

[21] **Acknowledgments.** L. De B. and G.S. O'B. were part funded by the department of Communications, Energy and Natural Resources (Ireland) under the National Geosciences programme 2007–2013. Financial assistance for field work from University College Dublin and the EU VOLUME project, and computational facilities from SFI/HEA ICHEC are acknowledged. A particular thanks to M. Möllhoff, A. Braiden, J. Grangeon, P. Bascou, M. La Rocca, D. Galluzzo and S. Rapisarda for assistance in the field experiment.

References

Battaglia, J., J.-L. Got, and P. Okubo (2003), Location of long-period events below Kilauea Volcano using seismic amplitudes and accurate relative relocation, *J. Geophys. Res.*, *108*(B12), 2553, doi:10.1029/2003JB002517.

Bonaccorso, A., M. Aloisi, and M. Mattia (2002), Dike emplacement forerunning the Etna July 2001 eruption modeled through continuous tilt and GPS data, *Geophys. Res. Lett.*, *29*(13), 1624, doi:10.1029/2001GL014397.

Chouet, B. (1996), Long-period volcano seismicity: Its source and use in eruption forecasting, *Nature*, *380*, 309–316.

Falsaperla, S., E. Privitera, B. Chouet, and P. Dawson (2002), Analysis of long-period events recorded at Mount Etna (Italy) in 1992, and their relationship to eruptive activity, *J. Volcanol. Geotherm. Res.*, *114*, 419–440.

Kumagai, H., B. A. Chouet, and M. Nakano (2002), Waveform inversion of oscillatory signatures in long-period events beneath volcanoes, *J. Geophys. Res.*, *107*(B11), 2301, doi:10.1029/2001JB001704.

Lokmer, I., C. J. Bean, G. Saccorotti, and D. Patanè (2007a), Moment-tensor inversion of LP events recorded on Etna in 2004 using constraints obtained from wave simulation tests, *Geophys. Res. Lett.*, *34*, L22316, doi:10.1029/2007GL031902.

Lokmer, I., G. Saccorotti, B. D. Lieto, and C. J. Bean (2007b), Temporal evolution of long-period seismicity at Etna Volcano, Italy, and its relationship with the 2004–2005 eruption, *Earth Planet. Sci. Lett.*, *34*, 205–220.

Métaxian, J.-P., P. Lesage, and B. Valette (2002), Locating sources of volcanic tremor and emergent events by seismic triangulation: Application to Arenal volcano, Costa Rica, *J. Geophys. Res.*, *107*(B10), 2243, doi:10.1029/2001JB000559.

Michelini, A., and B. Bolt (1986), Application of the principal parameters method to the Coalinga, California, aftershocks sequence, *Bull. Seismol. Soc. Am.*, *76*, 409–420.

Napoli, R., G. Currenti, C. Del Negro, F. Greco, and D. Scandura (2008), Volcanomagnetic evidence of the magmatic intrusion on 13th May 2008 Etna eruption, *Geophys. Res. Lett.*, *35*, L22301, doi:10.1029/2008GL035350.

Patanè, D., G. Di Grazia, A. Cannata, P. Montalto, and E. Boschi (2008), Shallow magma pathway geometry at Mt. Etna volcano, *Geochem. Geophys. Geosyst.*, *9*, Q12021, doi:10.1029/2008GC002131.

Saccorotti, G., I. Lokmer, C. Bean, G. D. Grazia, and D. Patanè (2007), Analysis of sustained long-period activity at Etna Volcano, Italy, *J. Volcanol. Geotherm. Res.*, *160*, 340–354.

C. J. Bean, L. De Barros, I. Lokmer, and G. S. O'Brien, School of Geological Sciences, University College Dublin, Belfield, Dublin 4, Ireland. (louis.debarros@ucd.ie)

J.-P. Métaxian, LGIT, Université de Savoie, IRD, CNRS, F-73376 Chambéry CEDEX, France.

D. Patanè and L. Zuccarello, Sezione di Catania, Istituto Nazionale di Geofisica e Vulcanologia, Piazza Roma 2, I-95125 Catania, Italia.

G. Saccorotti, Sezione di Pisa, Istituto Nazionale di Geofisica e Vulcanologia, Via della Faggiola 32, I-56126 Pisa, Italia.